materials

MDPI

Article

Enhanced Electrochemical Performance Promoted by Tin in Silica Anode Materials for Stable and High-Capacity Lithium-Ion Batteries

Xuli Ding *, Daowei Liang and Hongda Zhao

School of Science, Jiangsu University of Science and Technology, 666 Changhui Road, Zhenjiang 212100, China; Leong1664988857@163.com (D.L.); zhd1787278660@163.com (H.Z.)

* Correspondence: xuliding@just.edu.cn

Abstract: Although the silicon oxide (SiO_2) as an anode material shows potential and promise for lithium-ion batteries (LIBs), owing to its high capacity, low cost, abundance, and safety, severe capacity decay and sluggish charge transfer during the discharge–charge process has caused a serious challenge for available applications. Herein, a novel 3D porous silicon oxide@Pourous Carbon@Tin (SiO_2@Pc@Sn) composite anode material was firstly designed and synthesized by freeze-drying and thermal-melting self-assembly, in which SiO_2 microparticles were encapsulated in the porous carbon as well as Sn nanoballs being uniformly dispersed in the SiO_2@Pc-like sesame seeds, effectively constructing a robust and conductive 3D porous Jujube cake-like architecture that is beneficial for fast ion transfer and high structural stability. Such a SiO_2@Pc@Sn micro-nano hierarchical structure as a LIBs anode exhibits a large reversible specific capacity ~520 mAh·g^{-1}, initial coulombic efficiency (ICE) ~52%, outstanding rate capability, and excellent cycling stability over 100 cycles. Furthermore, the phase evolution and underlying electrochemical mechanism during the charge–discharge process were further uncovered by cyclic voltammetry (CV) investigation.

Keywords: porous carbon; silica; tin; anode materials; lithium-ion batteries

Citation: Ding, X.; Liang, D.; Zhao, H. Enhanced Electrochemical Performance Promoted by Tin in Silica Anode Materials for Stable and High-Capacity Lithium-Ion Batteries. *Materials* **2021**, *14*, 1071. https://doi.org/10.3390/ma14051071

Academic Editor: Suzy Surblé

Received: 18 January 2021
Accepted: 9 February 2021
Published: 25 February 2021

1. Introduction

Lithium-ion batteries (LIBs) have been regarded as one of the critical energy storage technologies that can be widely used in portable electronics and grid-scale energy storage due to their high energy density and cycle longevity to make a fossil fuel-free environment possible [1–5]. With the advent of electric vehicles (EV) in recent years, the traditional commercialized LIBs are obviously insufficient to meet the requirement owning to their limited capacities. Therefore, it is highly desired for LIBs with higher energy and power densities as well as lower cost to be developed [6–8].

According to the working principle of LIBs, the electrode materials play a critical role in the further improvement of the battery performance [9–16]. High-capacity and low-cost materials have triggered vast interest in the past few years [15–21], which can bring great promise for next-generation LIBs with a higher price–performance ratio. Silica (SiO_2) has recently captured great attention as a promising candidate anode materials for LIBs because of its suitable working potential (~0.25 V vs. Li/Li$^+$), proper theoretical specific capacity (~1960 mAh·g^{-1}), lesser volume variation (~100%), and expanded cycling lifespan compared to silicon and other alloys [22–39]. In addition, SiO_2 is one of the most abundant materials on earth, and its environmentally friendly and low-cost nature further turns it into an alternative electrode material [25–30]. However, the development of SiO_2-based anode materials so far has been impeded due to its poor electrical conductivity and sluggish charge transfer kinetics. To overcome these limitations, extensive research efforts have been dedicated to the development of SiO_2-based composite materials and structures, such as carbon-coated SiO_2 particles [32,35,36], SiO_2/Cu polyacrylonitrile-C composite [33], Sn(SnO_2)–SiO_2/graphene nanocomposites [37], Bi_2S_3@SiO_2 core-shell

microwires [38], Ni/SiO_2 hierarchical hollow spheres [39], and so on [34,40]. Even though significant progress has been achieved, the commercialization of SiO_2-based anodes is still restricted by the low electrochemical activity. On the other hand, metallic tin (Sn) has a good electrical conductivity (8.7×10^6 S·m^{-1}) and low melting point (~232 °C). When used as an electrode material, it shows a high theoretical capacity of 994 mAh·g^{-1} with the formation of $Li_{4.4}Sn$ and fitting working potential (~0.5 V). However, the huge volume changes (~260%) it suffers during Li alloying/dealloying can always lead to rapid fading of capacity and subsequently poor cyclability [41–47].

Taking advantages of both SiO_2 and Sn, herein, a feasible tactics was developed to construct porous silicon oxide@Pourous Carbon@Tin (SiO_2@Pc@Sn) composites with tunable SiO_2 to Sn molar ratios to synergistically storage Li in both porous SiO_2 and Sn. The SiO_2@Pc@Sn composite was fabricated using a simple and scalable freezing-drying and low-temperature thermal-melting combined method. The obtained composites possessed several advantageous features: Firstly, the porous structure in the composites largely shortened the transport path for Li ions and provided the buffering space for volume change during the charging/discharging process; secondly, porous C (Pc) and SiO_2 provided a rigid skeleton with long cycle stability; thirdly, the presence of Sn and Pc could improve the electrical conductivity of the SiO_2-based electrode. The synergetic effect of porous SiO_2, Pc, and Sn nano-ball empowered the fabricated SiO_2@Pc@Sn composite electrodes to be competent to show good electrochemical performance, including a stable and long cycling life, low electrochemical impedance, and enhanced specific capacity, which demonstrated a fascinating potential as a promising anode for the next-generation LIBs.

2. Experimental Section

2.1. Preparation of SiO_2@Pc Composites Material

Diatomite (325 mesh, Sinopharm Chemical Reagent Co., Ltd. Shanghai, China) was ground for 10 h by a high-energy ball mill, then the sample was dispersed in the glucose aqueous solution by ultrasonic for 15 mi. After that, the freeze-drying process for 60 h was carried out, in which the mass ratio of SiO_2 to glucose was 1:1 (w/w). Then, the freeze-drying samples were transferred to a tube furnace and carbonized for 3 h at 500 °C in an Ar/H_2 gas environment to obtain SiO_2@Pc composites.

2.2. Preparation of SiO_2@Pc @Sn Composites Material

The previously obtained SiO_2@Pc from the above step was weighed at ratio of 1:1 (w/w) with Sn powders (325 mesh, Sinopharm Chemical ReagentCo., Ltd. Shanghai, China) and mixed fully. Then the mixture was transferred to a tubular furnace (OTF-1200X), and heated at a rate of 5 °C/min to 300 °C, keeping for 1 h in an Ar/H_2 protect gas. After that, the sample of SiO_2@Pc@Sn was obtained via rapid cooling.

2.3. Battery Assembly and Electrochemical Measurements

The Celgard 2320 (Shenzhen, China) film was used as a membrane and lithium foil as a pair electrode to conduct electrochemical experiments on the CR2032 (Shenzhen, China) coin battery. The experimental electrolyte was configured of 1.0 M $LiPF_6$ dissolved in ethylene carbonate (EC) and diethyl carbonate (DEC) by volume 1:1. The working electrode was composed of 70 wt.% active materials, 15 wt.% polyvinylidene fluoride (PVDF) binder, and 15 wt.% Super P. After fully mixing and grinding, the slurry was spread on the copper foil evenly, and then dried in an oven at 50 °C for 12 h. The battery was assembled in a glove box filled with Ar gas and the oxygen and water content below 1.0 PPM. After assemblage, the batteries were set aside for 8 h at room temperature. The electrochemical performance was tested by electrochemical impedance spectroscopy (EIS) and cyclic voltammetry (CV) on a DH7001 electrochemical workstation, and the scanning rate of CV was set in the range of 0.1–0.5 mV s^{-1} with an applied potential 2–0 V, and the frequency range for EIS measurement was set in 1.0 MHz–0.1 Hz. All batteries' simulation cycling and charge/discharge were conducted on a land battery cabinet (LAND

CT2001A, Wuhan, China). In the batteries' evaluation process, the cut-off voltage was 0.005 V vs Li/Li^+ for discharge and 1.5 V for charge. All specific capacity was calculated based on the proportion of the active material in the whole electrode.

2.4. Characterization

The morphology and structure of SiO_2@Pc@Sn were obtained by a field-emission scanning electron microscope (FESEM, JEOL JMS-7001-F, JEOL, Tokyo, Japan). The element mapping was measured by the EDS instrument equipped in the FESEM. The phase composition of the material was obtained by X'Pert PRO diffractometer (XRD, Shimadzu, Japan: XRD-6000, Cu–K radiation, 0.15406 nm, λ = 1.5406 Å), the measurement angle was between 10–80°, and the scanning rate was 10°/min. Raman spectroscopy was used to characterize the form of carbon, and the excited wavelength of the laser was 532 nm (Raman, InVia and Ntegra Spectra, Renishaw & NT-MDT, London, UK). The thermogravimetry (TG) analysis was performed by the vertical zero friction dilatometer L75VS Linseis (Selb, Germany) from 25 to 800 °C in air to calculate the carbon weight percent in the composite.

3. Results and Discussion

The preparation flow chart of the SiO_2@Pc@Sn composite is shown in Figure 1. As depicted in the schematic diagram, firstly, the SiO_2@Pc composite with a porous structure was prepared by the freeze-drying method, and secondly, the SiO_2@Pc@Sn composite was obtained via the low-temperature thermal melting and self-assembly process.

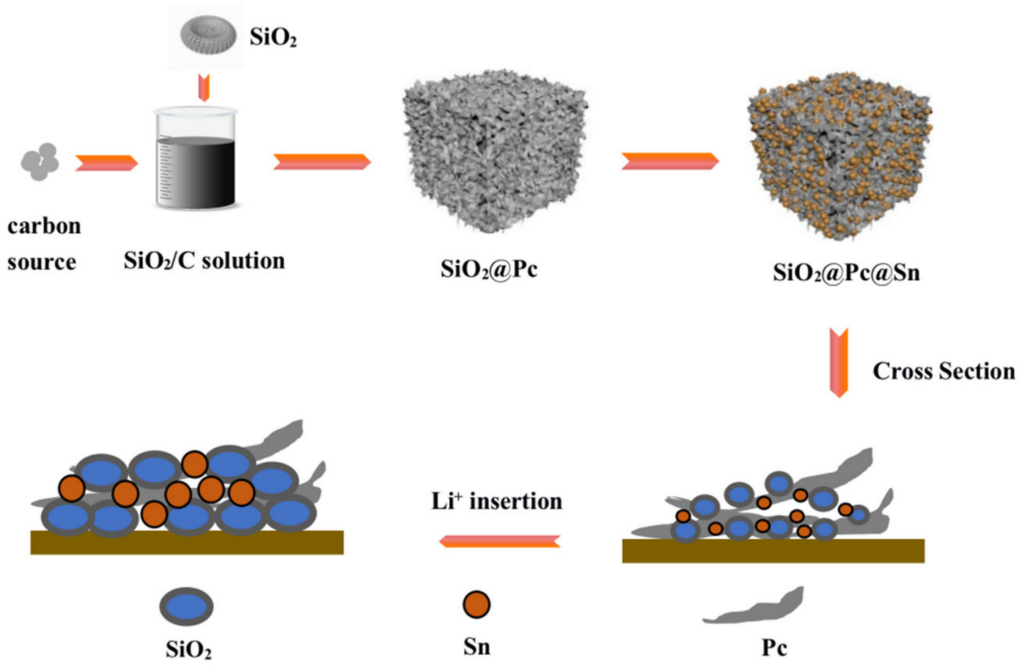

Figure 1. Schematic diagram of the synthesize process of silicon oxide@Pourous Carbon@Tin (SiO_2@Pc@Sn) composite.

Figure 2a shows the comparison of the XRD pattern of SiO_2, SiO_2@Pc, SiO_2@Pc@Sn, and PDF card of standard XRD, correspondingly. The characteristic peaks at 21.6° and 35.6° belonged to SiO_2 [26], and the peak value of SiO_2@Pc was consistent with that of SiO_2, indicating that SiO_2 did not change significantly after Pc coating. In the SiO_2@Pc@Sn composite, the characteristic peaks for Sn were centered at 30.6°, 32.1°, 43.9°, 44.9°, and 55.3°. The characteristic peaks that belonged to SiO_2 and Sn in the SiO_2@Pc@Sn composite were matched well with the standard PDF cards. The synthesized Pc was characterized by the Raman spectrum as indicated in Figure 2. It can be seen that the peaks around 1357 and 1591 cm^{-1} corresponded to the disordered D peak and graphitized G peak for the obtained

Pc. The D peak was generally the crystallization defect of carbon atoms and the G peak represented the in-plane vibration of sp^2 hybridization of carbon atoms [48,49]. The existence of the G peak and D peak indicates that the microstructure of Pc in the SiO_2@Pc@Sn composite was graphitized carbon. In addition, the main peak of SiO_2 at 480–490 cm^{-1} was not present in the current Raman spectrum 500–3000 cm^{-1} [27], while the peak around 1080 cm^{-1} under D peak of carbon was also invisible due to the encapsulation of SiO_2 in a carbon shell [26]. From the TG analysis result in the Raman spectrum, the C weight percent in the SiO_2@Pc composite was ~27.3%.

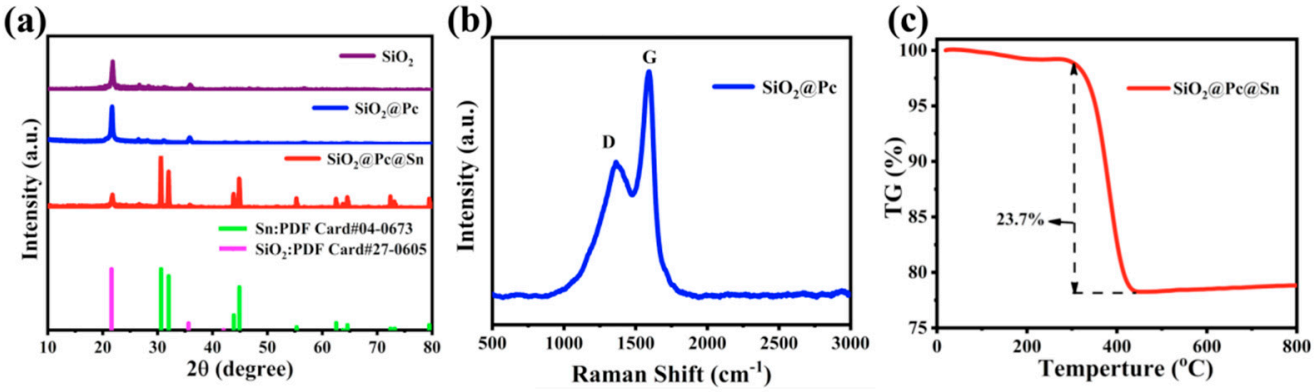

Figure 2. (**a**) XRD patterns of different samples; (**b**) Raman spectrum of SiO_2@Pc; (**c**) thermogravimetry (TG) diagram for the SiO_2@Pc.

The morphology and elements distribution of the obtained SiO_2@Pc@Sn composite was measured by scanning electron microscopy (SEM). As shown in Figure 3, the pristine SiO_2 was in the shape of a sunflower (Figure 3a), and its average size was between 20–40 μm, with many nano-pores on the surface (Figure 3b). The size of the pores was in the range of 50–600 nm (Figure 3b). From the images as shown in Figure 3c, after rapid cooling, the Sn nano-balls were formed and dispersed uniformly in the SiO_2@Pc composite, which filled into the pores in Pc or embedded among the SiO_2@Pc blocks. As shown in Figure 3f, the statistical distribution of size for the Sn balls was mainly centered around 100 nm. The element mapping for Si, Sn, and C in the SiO_2@Pc@Sn composite is shown in Figure 3g–i. From the result, it is found that three elements are distributed in all the areas detected in the SiO_2@Pc@Sn.

The electrochemical performance is displayed in Figure 4. The charge/discharge curves of different samples at the same current density of 100 $mA{\cdot}g^{-1}$ are compared in Figure 4a. It was found that the first discharge capacity reached to 1228 for SiO_2@Pc@Sn, 990 for SiO_2@Pc, 672 for bare SiO_2, and 352 $mA{\cdot}h{\cdot}g^{-1}$ for the synthesized Pc. The initial coulomb efficiency (ICE) was 52%, 37.7%, 29.9%, and 27.4%, respectively. The improved specific capacity and ICE of SiO_2@Pc@Sn were attributed to the fact that Pc and Sn can improve the electrical conductivity of the composite and enhance the electrochemical activity of SiO_2. The poor conductivity of SiO_2 was the cause of the low initial coulombic efficiency, and most of Li ions combined with SiO_2 to produce irreversible Li_4SiO_4 and Li_2O at the first charge and discharge [50,51], while the presence of Pc and Sn improved the whole electrical conductivity of SiO_2@Pc@Sn, which is helpful for the electrons to arrive at the surface of SiO_2, and as a result, facilitated the Li ions transfer in the composite. Meanwhile, the existence of Pc further prevented the by-products brought by the direct reaction between electrolyte and SiO_2 and Sn, thus improving the ICE of the composite [52]. The cycling performance at 100 $mA{\cdot}g^{-1}$ is compared in Figure 4b. It is evident that SiO_2@Pc@Sn shows the highest specific capacity and best capacity retention through 100 cycles. While for bare SiO_2, the capacity underwent continuous increasing during the initial 100 cycles that changed from the initial 200 to 400 $mA{\cdot}h{\cdot}g^{-1}$ after 100 cycles. Though the capacity of SiO_2@Pc could not reach SiO_2@Pc@Sn, it was still better than bare SiO_2 and

Pc. Moreover, the rate capability for different samples was listed in Figure 4c. It is clear that the SiO_2@Pc@Sn exhibited capacities of 650, 610, 580, and 520 $mA{\cdot}h{\cdot}g^{-1}$ at 100, 200, 500, and 1000 $mA{\cdot}g^{-1}$, respectively, whereas the bare SiO_2 and SiO_2@Pc exhibited a lower capacity and faster capacity decay. Obviously, the rate capability of SiO_2@Pc@Sn was better than that of the others, especially at high current density due to the fact that Pc and Sn had better conductivity than SiO_2, which provided higher mobility for Li ion diffusion through the whole electrode. Without the addition of other assistance, such as an electrolyte additive (for instance, FEC) and so on, the good rate capability and stable cycling performance of SiO_2@Pc@Sn was believed to be originated from the unique structure. Firstly, the built-in void in Pc and SiO_2 shorted the Li ions transfer distance in the electrode; secondly, Sn and Pc were conductive for electrons and ions, and the face-to-face contact between Pc and SiO_2 as well as Sn aroused more efficient channels for fast transfer of electrons and Li ions [15,17]. The CV test could detect electrode surface reaction process, electrochemical activity, and reversibility of the active material. Figure 4d is the CV curve of SiO_2@Pc@Sn. As shown, the cathode peak of 0.98 V in the first cathode scan was caused by electrolyte decomposition and the generation of the SEI layer [50], while the reductive peaks at 0.63 and 0.32 V were attributed to the phase Li_xSiO_y and Li_xSi formed while SiO_2 was combined with Li^+ in the discharge process [30,40]. On the contrary, the oxidation peaks at 0.64, 0.74, and 0.82 V were caused by the dealloying process of Li_xSn and $Li_2Si_2O_5$ [53].

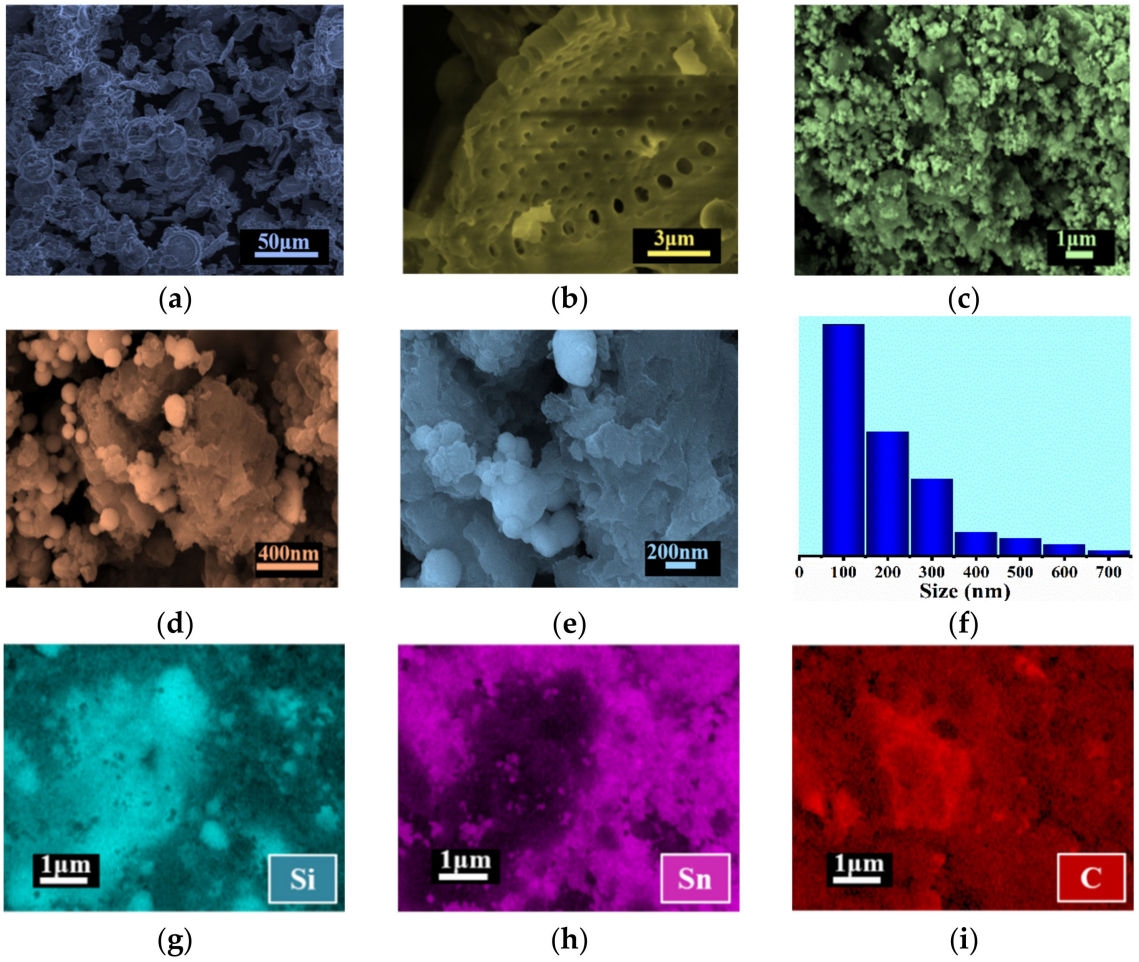

Figure 3. (**a**,**b**) SEM of bare SiO_2 with different magnification; (**c**–**e**) SEM of SiO_2@Pc@Sn with different magnification; (**f**) size distribution for Sn in the SiO_2@Pc@Sn composite; (**g**,**i**) element mapping of SiO_2@Pc@Sn for Si (**g**); Sn (**h**); and C (**i**).

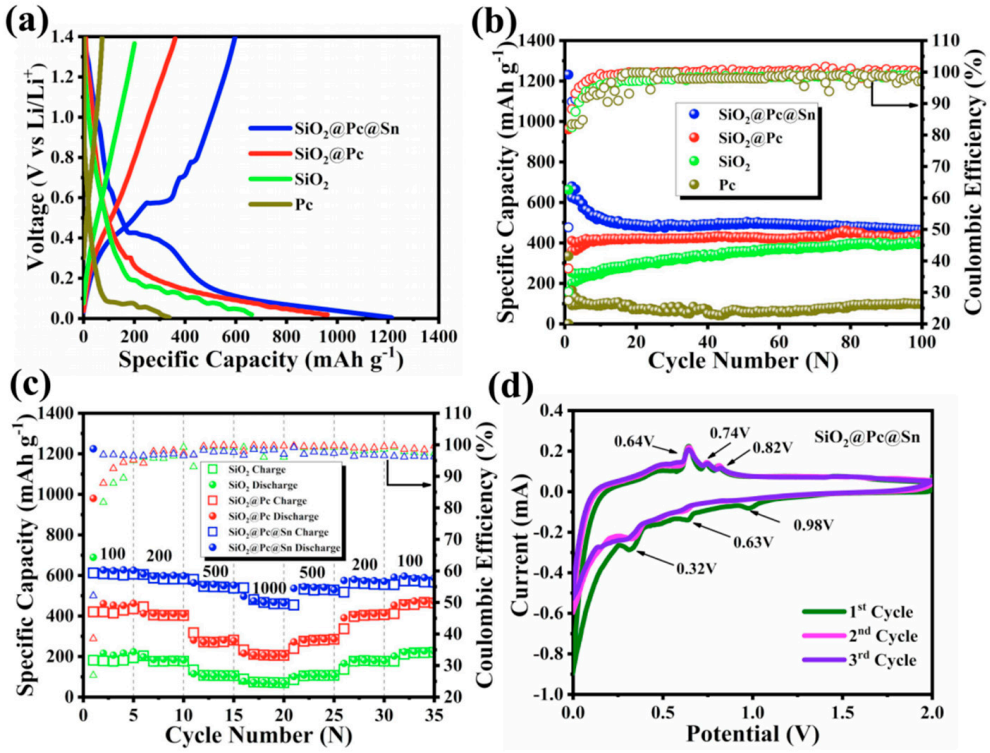

Figure 4. (**a**) Charge/discharge curve of different samples; (**b**) cycling performance curve of different samples; (**c**) the rate performance for different samples; (**d**) cyclic voltammetry (CV) curve of SiO_2@Pc@Sn.

Furthermore, the electrochemical impedance spectra (EIS) were compared and analyzed in Figure 5. From the Nyquist plots diagram of different samples, as shown in Figure 5a, it was found that all impedance spectra consisted of a semicircle in the high frequency region and an inclined line in the low frequency region, which corresponded to the Li^+ migration resistance and interface contact resistance in the active materials, respectively [54,55]. The impedance resistance was 205 for bare SiO_2, 129 for the SiO_2@Pc, and 77 Ω for SiO_2@Pc@Sn, indicating that the migration impedance of Li ions was minimal in the active material of SiO_2@Pc@Sn. In addition, EIS was often used in the qualitative determination of Li ions' diffusion coefficient in LIB materials. Figure 5b is the plots of correlation curve of Z_{re} (real part of impedance) and $w^{-1/2}$ (w is the frequency) within the frequency range of 1–0.1 Hz for the electrode composed of different materials. According to the relation, $Z_{re} = G - k \cdot w^{-1/2}$, where, k is the slope of the correlation curve between Z_{re} and $w^{-1/2}$, from which the diffusion coefficient of lithium ions in different electrode materials can be qualitatively deduced [20]. In order to ensure the accuracy of the experiment, each set of data tested 5–10 batteries for analysis. From the fitting results (Figure 5b), the curve slopes k of SiO_2, SiO_2@Pc, and SiO_2@Pc@Sn were 0.33, 0.20 and 0.07, respectively. The result showed that the diffusion coefficient of Li^+ was the largest in the SiO_2@Pc @Sn composite according to the relation formula [21], $D_{Li+} = A/k$, where, A is constant related to the Li ions content and electrode area, etc.

Meanwhile, the CV measurement with different scanning rates ($mV \cdot s^{-1}$) is shown in Figure 6. The CV curves of SiO_2 (Figure 6a), SiO_2@Pc (Figure 6b), and SiO_2@Pc@Sn (Figure 6c) electrodes under scanning rates of 0.1, 0.2, 0.3, 0.4, and 0.5 $mV \cdot s^{-1}$ were measured. The obtained peak current I_{max} and the quadratic root of scanning rate $v^{1/2}$ were fitted linearly, from which the diffusion strength of Li^+ in different electrode materials could be qualitatively determined. According to the Randle–Sevcik equation: $I_{max} = Av \cdot^{1/2} \cdot D_{oLi}$ [56], where A is the constant related to charge and surface area, v is the scanning rate of CV, and D_{oLi} is the diffusion coefficient of Li^+ in oxide [54]. According to

the test results shown in Figure 6d, the slopes were 0.49, 0.44, and 0.12 for SiO_2@Pc@Sn, SiO_2@Pc, and bare SiO_2, respectively, indicating that the diffusion coefficient of Li^+ ions was the highest in SiO_2@Pc@Sn compared with the two others [57]. The result was also consistent with the fitting results of the correlation curve between Z_{re} and $v^{-1/2}$ of EIS in the frequency range of 1–0.1 Hz (Figure 5b), which further demonstrated that Sn could improve the electrochemical performance of SiO_2-based anode materials for LIBs.

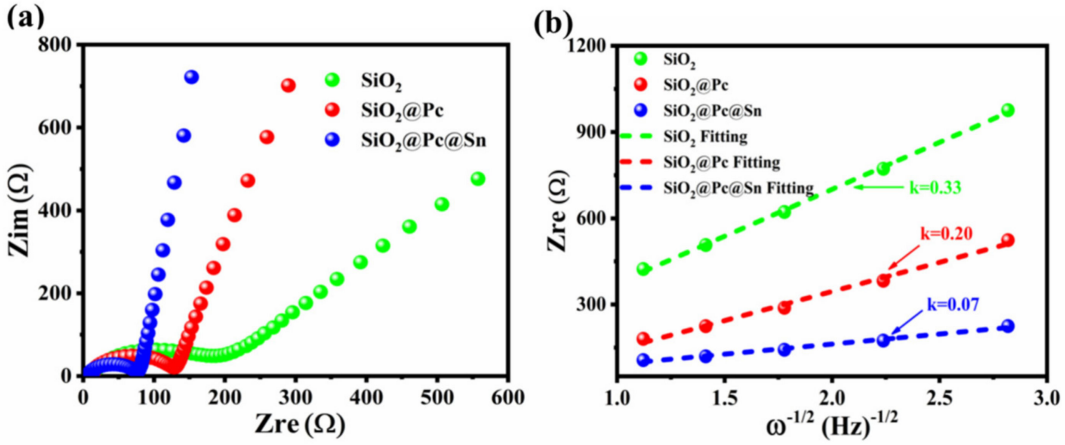

Figure 5. (**a**) Comparison for the Nyquist diagram of different samples; (**b**) impedance real part Z_{re} Vs $w^{-1/2}$ in the frequency range 1–0.1 Hz.

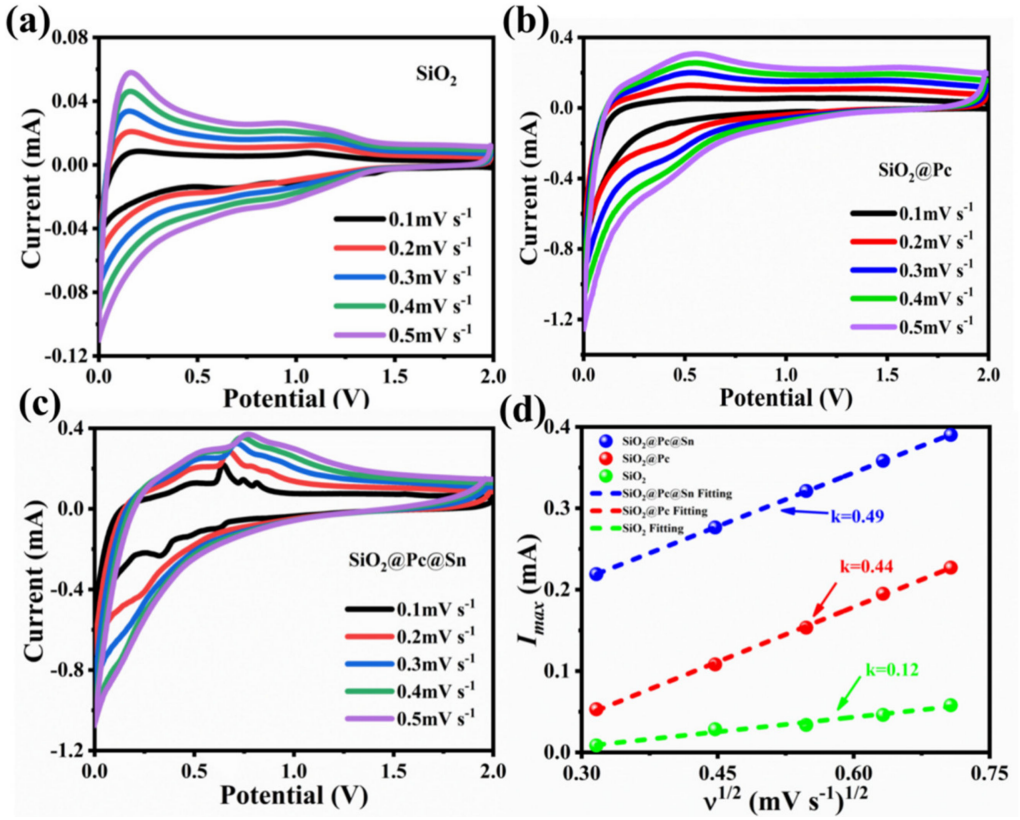

Figure 6. (**a**–**c**) CV curve of SiO_2, SiO_2@Pc, and SiO_2@Pc@Sn with different scanning rates of 0.1–0.5 mV·s^{-1}; (**d**) relationship between scan rate and peak current.

4. Summary

The SiO_2@Pc@Sn composite anode material was prepared by the freeze-drying and low-temperature thermal melting method, which exhibited improved electrochemical performance and faster Li^+ transfer kinetic. The synergetic effect of porous carbon, SiO_2, and Sn endows the as-fabricated SiO_2@Pc@Sn composites to be competent to show good electrochemical performance. When used as an anode in LIBs, the SiO_2@Pc@Sn composite could deliver a large reversible capacity of 650 at 100 $mA \cdot g^{-1}$, a remarkable rate capability of 500 retained at 1000 $mA \cdot g^{-1}$, and a long-term cycling durability with ~87% capacity retention over 100 cycles. EIS and CV measurements demonstrated that, with the participation of Sn phase and Pc, the diffusion and migration kinetics of Li ions in SiO_2@Pc@Sn composites was significantly improved. The understanding of the synergistic effect of Li storage between SiO_2 and Sn in this work will not only provide insight towards exploring new SiO_2-based anode materials, but also shed light on the design of other low-cost and environmentally friendly electrode materials for the next-generation LIBs.

Author Contributions: Conceptualization, X.D.; methodology, X.D.; software, D.L.; validation, X.D., D.L. and H.Z.; formal analysis, X.D. and D.L.; investigation, X.D., D.L.; resources, X.D.; data curation, D.L., H.Z.; writing—original draft preparation, X.D.; writing—review and editing, X.D.; visualization, X.D., D.L. and H.Z.; supervision, X.D.; project administration, X.D.; funding acquisition, X.D. All authors have read and agreed to the published version of the manuscript.

Funding: This work was supported by the National Natural Science Foundation of China (No.11874282, 11604245, 11981240429), the Six Talent Peaks Project in Jiangsu Province (No. 2019-XNY-074), the Vice President Project of Industry-University-Research Cooperation in Science and Technology of Jiangsu Province (No. BY2020675).

Institutional Review Board Statement: Not applicable.

Informed Consent Statement: Not applicable.

Data Availability Statement: Data sharing not applicable.

Conflicts of Interest: The authors declare no conflict of interest.

References

1. Zhang, J.-N.; Li, Q.; Ouyang, C.; Yu, X.; Ge, M.; Huang, X.; Hu, E.; Ma, C.; Li, S.; Xiao, R.; et al. Trace doping of multiple elements enables stable battery cycling of LiCoO2 at 4.6 V. *Nat. Energy* **2019**, *4*, 594–603. [CrossRef]
2. Yang, C.; Ji, X.; Fan, X.; Gao, T.; Suo, L.; Wang, F.; Sun, W.; Chen, J.; Chen, L.; Han, F.; et al. Flexible Aqueous Li-Ion Battery with High Energy and Power Densities. *Adv. Mater.* **2017**, *29*. [CrossRef] [PubMed]
3. Yang, H.; Wu, H.-H.; Ge, M.; Li, L.; Yuan, Y.; Yao, Q.; Chen, J.; Xia, L.; Zheng, J.; Zhao, Y.; et al. Simultaneously Dual Modification of Ni-Rich Layered Oxide Cathode for High-Energy Lithium-Ion Batteries. *Adv. Funct. Mater.* **2019**, *29*, 1808–1825. [CrossRef]
4. Li, L.; Fang, C.; Wei, W.; Zhang, L.; Ye, Z.; He, G.; Huang, Y. Nano-ordered structure regulation in delithiated Si an-ode triggered by homogeneous and stable Li-ion diffusion at the interface. *Nano Energy* **2020**, *72*, 104651. [CrossRef]
5. Han, M.; Yu, J. Subnanoscopically and homogeneously dispersed SiOx/C composite spheres for high-performance lithium ion battery anodes. *J. Power Sources* **2019**, *414*, 435–443. [CrossRef]
6. Doughty, D.H.; Crafts, C.C. *FreedomCAR Electrical Energy Storage System Abuse Test Manual for Electric and Hybrid Electric Vehicle Applications*; Sandia Report SAND2005-3123; Sandia National Laboratories: Albuquerque, NM, USA; Livermore, CS, USA, 2006.
7. Commission NDAR, QC/T-743-2006. Automotive standard of the People's Republic of China: Lithium Ion Bateries for Electric Vehicles. 2006. Available online: https://max.book118.com/html/2017/0726/124432928.shtm (accessed on 13 February 2021).
8. Perner, A.; Vetter, J. Lithium-ion batteries for hybrid electric vehicles. In *Advances in Battery Technologies for Electric Vehicles*; Elsevier BV: Amsterdam, The Netherlands, 2015; pp. 173–190.
9. Cabana, J.; Monconduit, L.; Larcher, D.; Palacín, M.R. Beyond Intercalation-Based Li-Ion Batteries: The State of the Art and Challenges of Electrode Materials Reacting Through Conversion Reactions. *Adv. Mater.* **2010**, *22*, E170–E192. [CrossRef]
10. Whittingham, M.S. ChemInform Abstract: Ultimate Limits to Intercalation Reactions for Lithium Batteries. *ChemInform* **2015**, *114*, 11414–11443. [CrossRef]
11. Zhang, Q.; Uchaker, E.; Candelaria, S.L.; Cao, G. ChemInform Abstract: Nanomaterials for Energy Conversion and Storage. *Cheminform* **2013**, 44. [CrossRef]
12. Masquelier, C.; Croguennec, L. Polyanionic (Phosphates, Silicates, Sulfates) Frameworks as Electrode Materials for Rechargeable Li (or Na) Batteries. *Chem. Rev.* **2013**, *113*, 6552–6591. [CrossRef] [PubMed]

13. Song, H.-K.; Lee, K.T.; Kim, M.G.; Nazar, L.F.; Cho, J. Recent Progress in Nanostructured Cathode Materials for Lithium Secondary Batteries. *Adv. Funct. Mater.* **2010**, *20*, 3818–3834. [CrossRef]
14. Jia, H.; Gao, P.; Yang, J.; Wang, J.; Nuli, Y.; Yang, Z. Novel Three-Dimensional Mesoporous Silicon for High Power Lithium-Ion Battery Anode Material. *Adv. Energy Mater.* **2011**, *1*, 1036–1039. [CrossRef]
15. Ding, X.; Liu, X.; Huang, Y.; Zhang, X.; Zhao, Q.; Xiang, X.; Li, G.; He, P.; Wen, Z.; Li, J.; et al. Enhanced electrochemical performance promoted by monolayer graphene and void space in silicon composite anode materials. *Nano Energy* **2016**, *27*, 647–657. [CrossRef]
16. Tao, W.; Wang, P.; You, Y.; Park, K.; Wang, C.-Y.; Li, Y.-K.; Cao, F.-F.; Xin, S. Strategies for improving the storage per-formance of silicon-based anodes in lithium-ion batteries. *Nano Res.* **2019**, *12*, 1739–1749. [CrossRef]
17. Ding, X.; Wang, Y. Bilayer-graphene-coated Si nanoparticles as advanced anodes for high-rate lithium-ion bat-teries. *Electrochim. Acta* **2020**, *329*, 134975. [CrossRef]
18. Luo, J.; Tao, X.; Zhang, J.; Xia, Y.; Huang, H.; Zhang, L.; Gan, Y.; Liang, C.; Zhang, W. Sn4+ Ion Decorated Highly Conductive Ti3C2 MXene: Promising Lithium-Ion Anodes with Enhanced Volumetric Capacity and Cyclic Performance. *ACS Nano* **2016**, *10*, 2491–2499. [CrossRef]
19. Ding, X.; Wang, H.; Liu, X.; Gao, Z.; Huang, Y.; Lv, D.; He, P.; Huang, Y. Advanced anodes composed of graphene encapsulated nano-silicon in a carbon nanotube network. *Rsc Adv.* **2017**, *7*, 15694–15701. [CrossRef]
20. Li, W.; Feng, X.; Chen, Y. High performance lithium battery anode materials by coating SiO_2 nanowire arrays with PEO. *New J. Chem.* **2019**, *43*, 14609–14615. [CrossRef]
21. Yi, X.; Yu, W.J.; Tsiamtsouri, M.A.; Zhang, F.; He, W.; Dai, Q.; Hu, S.; Tong, H.; Zheng, J.; Zhang, B. Highly conductive C-Si@G nanocomposite as a high-performance anode material for Li-ion batteries. *Electrochim. Acta* **2018**, *295*, 295. [CrossRef]
22. Liu, Y.; Jing, S.X.; Luo, S.H.; Li, S.H. Silicon oxides: A promising family of anode materials for lithium-ion batteries. *Nat. Prod. Rep.* **2019**, *36*, 626–665. [CrossRef] [PubMed]
23. Tang, C.; Liu, Y.; Xu, C.; Zhu, J.; Wei, X.; Zhou, L.; He, L.; Yang, W.; Mai, L. Ultrafine Nickel-Nanoparticle-Enabled SiO_2 Hierarchical Hollow Spheres for High-Performance Lithium Storage. *Adv. Funct. Mater.* **2018**, *28*, 1704561. [CrossRef]
24. Favors, Z.; Wang, W.; Bay, H.H.; George, A.; Ozkan, M.; Ozkan, C.S. Stable cycling of SiO_2 nanotubes as high-performance anodes for lithium-ion batteries. *Sci. Rep.* **2014**, *4*, 4605.
25. Chang, W.-S.; Park, C.-M.; Kim, J.-H.; Kim, Y.-U.; Jeong, G.; Sohn, H.-J. Quartz (SiO_2): A new energy storage anode mate-rial for Li-ion batteries. *Energy Environ. Sci.* **2012**, *5*, 6895. [CrossRef]
26. Meng, J.; Cao, Y.; Suo, Y.; Liu, Y.; Zhang, J.; Zheng, X. Facile Fabrication of 3D SiO_2@Graphene Aerogel Composites as Anode Material for Lithium Ion Batteries. *Electrochim. Acta* **2015**, *176*, 1001–1009. [CrossRef]
27. Ichikawa, S.; Suda, J.; Sato, T.; Suzuki, Y. Lattice dynamics and temperature dependence of the first-order Raman spectra for? SiO_2 crystals. *J. Raman Spectrosc.* **2003**, *34*, 135–141. [CrossRef]
28. Brijesh, K.; Dhanush, P.C.; Vinayraj, S.; Nagaraja, H.S. Monoclinic Wolframite ZnWO4/SiO_2 nanocomposite as an anode material for lithium ion battery. *Mater. Lett.* **2020**, *275*, 128108.
29. Di, F.W.; Wang, N.; Li, L.X.; Geng, X.; Yang, H.M.; Zhou, W.M.; Sun, C.G.; An, B.G. Coral-like porous composite material of silicon and carbon synthesized by using diatomite as self-template and precursor with a good performance as an-ode of lithium-ions battery. *J. Alloy. Compd.* **2021**, *854*. [CrossRef]
30. Shen, D.; Huang, C.; Gan, L.; Liu, J.; Gong, Z.; Long, M. Rational Design of Si@SiO_2/C Composites Using Sustainable Cellulose as a Carbon Resource for Anodes in Lithium-Ion Batteries. *ACS Appl. Mater. Interfaces* **2018**, *10*, 7946–7954. [CrossRef]
31. Dong, X.; Zheng, X.; Deng, Y.; Wang, L.; Ju, Z. SiO_2/N-doped graphene aerogel composite anode for lithium-ion batteries. *J. Mater. Sci.* **2020**, *55*, 13023–13035. [CrossRef]
32. Yao, Y.; Zhang, J.; Xue, L.; Huang, T.; Yu, A. Carbon-coated SiO_2 nanoparticles as anode material for lithium ion bat-teries. *J. Power Sources* **2011**, *196*, 10240–10243. [CrossRef]
33. Li, M.; Li, J.; Li, K.; Zhao, Y.; Zhang, Y.; Gosselink, D.; Chen, P. SiO_2/Cu/polyacrylonitrile-C composite as anode mate-rial in lithium ion batteries. *J. Power Sources* **2013**, *240*, 659–666. [CrossRef]
34. Li, W.; Wang, F.; Ma, M.; Zhou, J.; Liu, Y.; Chen, Y. Preparation of SiO_2 nanowire arrays as anode material with en-hanced lithium storage performance. *RSC Adv.* **2018**, *8*, 33652–33658. [CrossRef]
35. Liang, Y.; Cai, L.; Chen, L.; Lin, X.; Fu, R.; Zhang, M.Q.; Wu, D. Silica nanonetwork confined in nitrogen-doped ordered mesoporous carbon framework for high-performance lithium-ion battery anodes. *Nanoscale* **2015**, *7*, 3971–3975. [CrossRef]
36. Pang, H.; Zhang, W.; Yu, P.; Pan, N.; Hu, H.; Zheng, M.; Xiao, Y.; Liu, Y.; Liang, Y. Facile Synthesis of Core-Shell Structured SiO_2@Carbon Composite Nanorods for High-Performance Lithium-Ion Batteries. *Nanomaterials* **2020**, *10*, 513. [CrossRef] [PubMed]
37. Namsar, O.; Autthawong, T.; Laokawee, V.; Boonprachai, R.; Haruta, M.; Kurata, H.; Yu, A.; Chairuangsri, T.; Sarakonsri, T. Improved electrochemical performance of anode materials for high energy density lithium-ion batteries through Sn(SnO_2)–SiO_2/graphene-based nanocomposites prepared by a facile and low-cost approach. *Sustain. Energy Fuels* **2020**, *4*, 4625–4636. [CrossRef]
38. Tang, C.; Li, N.; Sheng, J.; Zhou, L.; He, L.; Zhu, J.; Li, F.; Liu, Y.; Mai, L. Facile Synthesis of Bi2S3@SiO_2 Core-Shell Microwires as High-Performance Anode Materials for Lithium-Ion Batteries. *J. Electrochem. Soc.* **2017**, *164*, 6110–6115. [CrossRef]

39. Tu, J.; Yuan, Y.; Zhan, P.; Jiao, H.; Wang, X.; Zhu, H.; Jiao, S. Straightforward Approach toward SiO_2 Nanospheres and Their Superior Lithium Storage Performance. *J. Phys. Chem. C* **2014**, *118*, 7357–7362. [CrossRef]
40. Liu, D.D.; Kong, Z.; Liu, X.H.; Fu, A.P.; Wang, Y.Q.; Guo, Y.G.; Guo, P.Z.; Li, H.L.; Zhao, X.S. Spray-Drying induced assembly of skeleton-structured SnO_2/Graphene composite spheres as superior anode materials for high-performance lithium-ion batteries. *ACS Appl. Mater. Inter.* **2018**, *10*, 2515–2525. [CrossRef]
41. Xin, F.; Whittingham, M.S. Challenges and Development of Tin-Based Anode with High Volumetric Capacity for Li-Ion Batteries. *Electrochem. Energy Rev.* **2020**, *3*, 643–655. [CrossRef]
42. Wang, K.; He, X.; Ren, J.; Jiang, C.; Wan, C. Preparation of Sn/C microsphere composite anode for lithium-ion batteries via carbonthermal reduction. *Electrochem. Solid St.* **2006**, *9*, 320–323.
43. Derrien, G.; Hassoun, J.; Panero, S.; Scrosati, B. Nanostructured Sn–C Composite as an Advanced Anode Material in High-Performance Lithium-Ion Batteries. *Adv. Mater.* **2007**, *19*, 2336–2340. [CrossRef]
44. Zhao, X.; Wang, W.; Hou, Z.; Yu, Y.; Di, Q.; Wu, X.; Wei, G.; Quan, Z.; Zhang, J. Monodisperse tin nanoparticles and hollow tin oxide nanospheres as anode materials for high performance lithium ion batteries. *Inorg. Chem. Front.* **2018**, *6*, 473–476. [CrossRef]
45. Tolosa, A.; Widmaier, M.; Krüner, B.; Griffin, J.M.; Presser, V. Continuous silicon oxycarbide fiber mats with tin nanoparticles as high capacity anode for lithium-ion batterie. *Sustain. Energy Fuels* **2018**, *2*, 215–228.
46. Huang, X.; Cui, S.; Chang, J.; Hallac, P.B.; Fell, C.R.; Luo, Y.; Metz, B.; Jiang, J.; Hurley, P.T.; Chen, J. A Hierarchical Tin/Carbon Composite as an Anode for Lithium-Ion Batteries with a Long Cycle Life. *Angew. Chem. Int. Ed.* **2014**, *54*, 1490–1493. [CrossRef] [PubMed]
47. Yan, Y.; Ben, L.; Zhan, Y.; Huang, X. Nano-Sn embedded in expanded graphite as anode for lithium ion batteries with improved low temperature electrochemical performance. *Electrochim. Acta* **2016**, *187*, 186–192. [CrossRef]
48. Zhao, Y.; Liu, Z.; Zhang, Y.; Mentbayeva, A.; Wang, X.; Maximov, M.Y.; Liu, B.; Bakenov, Z.; Yin, F. Facile Synthesis of SiO_2@C Nanoparticles Anchored on MWNT as High-Performance Anode Materials for Li-ion Batteries. *Nanoscale Res. Lett.* **2017**, *12*, 1–7. [CrossRef] [PubMed]
49. Wu, W.; Liang, Y.; Ma, H.; Peng, Y.; Yang, H. Insights into the conversion behavior of SiO-C hybrid with pre-treated graphite as anodes for Li-ion batteries. *Electrochim. Acta* **2016**, *187*, 473–479. [CrossRef]
50. Ma, B.; Luo, J.; Deng, X.; Wu, Z.; Luo, Z.; Wang, X.; Wang, Y. Hollow Silicon–Tin Nanospheres Encapsulated by N-Doped Carbon as Anode Materials for Lithium-Ion Batteries. *ACS Appl. Nano Mater.* **2018**, *1*, 6989–6999. [CrossRef]
51. Blanco, M.V.; Renman, V.; Vullum-Bruer, F.; Svensson, A.M. Nanostructured diatom earth SiO_2 negative electrodes with superior electrochemical performance for lithium ion batteries. *RSC Adv.* **2020**, *10*, 33490–33498. [CrossRef]
52. Ma, B.; Lu, B.; Luo, J.; Deng, X.; Wu, Z.; Wang, X. The hollow mesoporous silicon nanobox dually encapsulated by SnO_2/C as anode material of lithium ion battery. *Electrochim. Acta* **2018**, *288*, 61–70. [CrossRef]
53. Gu, Z.; Xia, X.; Liu, C.; Hu, X.; Chen, Y.; Wang, Z.; Liu, H. Yolk structure of porous C/SiO_2 /C composites as. anode for lithium-ion batteries with quickly activated SiO_2. *J. Alloy. Compd.* **2018**, *757*, 265–272. [CrossRef]
54. Chen, S.; Shen, L.; Aken, P.v.A.; Maier, J.; Yu, Y. Dual-Functionalized Double Carbon Shells Coated Silicon Nanoparticles for High Performance Lithium-Ion Batteries. *Adv. Mater.* **2017**, *29*. [CrossRef]
55. He, Y.; Xu, G.; Wang, C.; Xu, L.; Zhang, K. Horsetail-derived Si@N-doped carbon as low-cost and long cycle life anode for Li-ion half/full cells. *Electrochim. Acta* **2018**, *264*, 173–182. [CrossRef]
56. Park, C.-K.; Park, S.-B.; Oh, S.-H.; Jang, H.; Cho, W.-I. Li Ion Diffusivity and Improved Electrochemical Performances of the Carbon Coated LiFePO 4. *Bull. Korean Chem. Soc.* **2011**, *32*, 836–840. [CrossRef]
57. Wang, H.; Yang, X.; Wu, Q.; Zhang, Q.; Chen, H.; Jing, H.; Wang, J.; Mi, S.-B.; Rogach, A.L.; Niu, C. Encapsulating Silica/Antimony into Porous Electrospun Carbon Nanofibers with Robust Structure Stability for High-Efficiency Lithium Storage. *ACS Nano* **2018**, *12*, 3406–3416. [CrossRef] [PubMed]